47th AIAA Aerospace Sciences Meeting Including The New Horizons Forum and Aerospace Exposition
5 - 8 January 2009, Orlando, Florida

AIAA 2009-1105

Numerical Study on Drag Reduction for Grid-Fin Configurations

Yan Zeng, Jinsheng Cai , Marco Debiasi, and Tat Loon Chng
National University of Singapore, Singapore, 119260, Singapore

A grid fin, or lattice fin, consists of an outer frame supporting an inner grid of intersecting planar surfaces of small chord. At transonic Mach numbers normal shocks form at the back of the lattice cells thus choking the flow through the cells and causing a significant increase in drag force. In order to reduce the transonic flow choking, an improved, sweptback grid fin configuration is proposed in the present study. Viscous computational fluid dynamic (CFD) simulations were performed to investigate the flow characteristics of a vehicle with baseline and sweptback grid fins at transonic and supersonic Mach numbers in the range 0.817- 2.0, at zero angle of attack. Good agreement (within the error of 4%) is observed for the computed drag coefficients with data available in literature. The present numerical results indicate the sweptback grid fins reduce the flow chocking. This translates in a grid-fin drag reduction of about 12% for all the Mach numbers investigated in the present study.

Nomenclature

C_p = pressure coefficient
C_D = overall vehicle drag coefficient
$C_{D,fin}$ = grid-fin drag coefficient
c = grid-fin chord (web element chord)
D = diameter (caliber) of the vehicle body
E = total energy
h = grid-fin height
H = total enthalpy
M = Mach number
M_∞ = freestream Mach number
Re_D = Reynolds number, $U_\infty D/\nu$
p = pressure
s = grid-fin span
t = time
w = thickness of the web elements
u_i = velocity vector
U_∞ = freestream velocity
w = thickness of the web elements
x_i = position vector

Greek letters
γ = ratio of specific heats
Λ = sweptback angle
μ = dynamic viscosity
ν = kinematic viscosity
ρ = flow density

I. Introduction

A grid fin, also called a lattice fin, is an unconventional aerodynamic control device consisting of an outer frame with internal intersecting grid frameworks of small chord. Unlike conventional fins that are aligned parallel to the direction of the airflow, a grid fin is arranged perpendicular to the flow allowing the oncoming air to pass through the lattice grid cells. The improved maneuverability offered by grid fins at high supersonic speeds and high angles of attack has attracted much attention to grid fins in recent years.

Flow passing through grid fins is quite complex due to their complicated configurations. Thus computational methods are considered as useful tools to solve the complete flow field. Recently more research efforts have been taken to investigate the aerodynamic characteristics of these devices in order to optimize their performance by using computational fluid dynamics (CFD) analysis.

Chen et al. [1] conducted numerical investigations of an ogive-cylinder configuration with grid fins by using the NPARC code of NASA. Viscous flows can be laminar and/or turbulent with a number of turbulent models available. The implicit approximate factorization scheme proposed by Beam and Warming and the multi-step Runge-Kutta scheme proposed by Jameson are used for solving the Euler/Navier-Stokes equations. Owing to computational resource limitations, most of the grid fin solutions were obtained using the Euler option in NPARC. The topology of the multi-block structured grid fin was set up by using ICEM Mulcad module and then used for grid generation by the ICEM Padamm module. The issue of the grid fin size, in terms of both the panel thickness and the frontal shape was addressed by covering three thicknesses for the grid fin panel, having a simple blunt square face and a sharp knife-edge shape.

Later, Lin et al. [2, 3] performed computations of turbulent flows past a grid fin alone and fin/body combination shapes at Mach numbers of 2.5 and 0.7. Navier–Stokes equations with the Baldwin–Barth one-equation turbulence model were discretized into finite difference form and solved by an algorithm in a fully coupled, implicit, and large block structure. Structure grid was generated with an algorithm combining “block-off” and “multiblock” methods for the complex configurations. The computations provided the detailed flow fields including Mach-number contours, pressure contours, and streamline patterns as well as the integrated aerodynamic coefficients. Good agreements were obtained on the normal-force coefficient and the bending-moment coefficient up to larger angles of attack. However, except for small angles of attack, limited agreements were obtained on axial-force coefficient and hinge-moment coefficient.

An important aerodynamic characteristic of grid fins concerns drag, which could be an advantage or a disadvantage depending on the speed of the airflow. At low subsonic speeds, the drag and control effectiveness of a lattice fin are about the same as those of a conventional fin, as the thin shape of the lattice walls creates very little disturbance in the flow of air passing through. However, the same behavior does not hold true at Mach numbers near 1. In this transonic regime, the flow inside the cells chokes thus reducing the flow rate through the fin, and the lattice effectively acts as an obstacle to the flow. Due to the formation of normal shock waves, the drag increases significantly and the control effectiveness decreases. A recent computational fluid dynamics (CFD) study [4] was conducted to investigate the transonic flow from within and about the cells of a lattice grid tail fin vehicle by using FLUENT, commercial CFD software. The CFD results illustrated that a normal shock forms at the back of the lattice grid cells at transonic Mach numbers, resulting in the flow to choke with overall drag increased significantly. At higer speed, the normal shock is swallowed and shock waves are instead formed off the leading edges of the lattice with an oblique angle. The oblique angle decreases with increasing the Mach number until the shock passes through the structure without intersecting it. In this regime, the drag and the control effectiveness of grid fins are superior.

Thus the main objective of the present CFD study is to find a way to overcome the high drag of the grid fins in the transonic flow regime. An improved configuration, sweptback grid fins, is proposed to reduce the transonic choking without changing the control effectiveness of the grid fin. The physics of shock interaction and choking in the cells of baseline and sweptback grid fins are also studied under transonic and supersonic flows.

Starting with validation of the present numerical method, flows over a vehicle with baseline grid fins used by Orthner [4] are simulated, in transonic and supersonic flows with Mach number 0.8-2.0, at zero angle of attack. After method validation, the aerodynamic characteristics of a sweptback grid fin configuration and the flow fields for a vehicle with sweptback grid fins are numerically predicted under the same range of Mach numbers and zero angle of attack.

The subsequent part of this paper is organized in the following manner: section II provides a description of the numerical method used, followed by a presentation and discussion of the results in section III. Section IV provides the concluding remarks.

II. Numerical Approach

A. Grid fin configurations

The model investigated by Orthner [4] is selected as the baseline, which consists of an ogive-cylinder body of diameter *D* with a 3-*D* tangent ogive nose, 13-*D* long cylindrical afterbody with four grid fins mounted in a cruciform orientation, as shown in Figure 1. The pitch axis of the grid fins is located 1.5-*D* from the rear of the cylinder. The grid fin has rectangular shaped outer frames, with the span (*s*), height (*h*) and chord (*c*) of 0.75-, 0.333- and 0.118-*D* respectively. The web thickness (*w*) is 0.007-*D*.

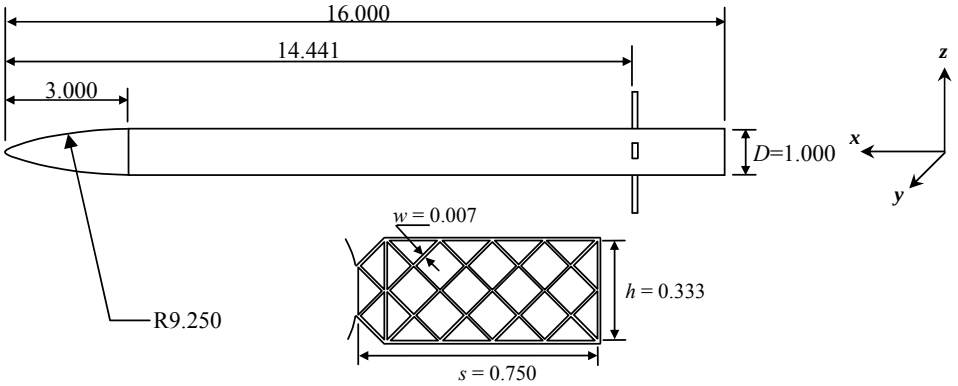

Figure 1. Schematic of the ogive cylinder with grid fin configuration (adapted from Ref. [4]).

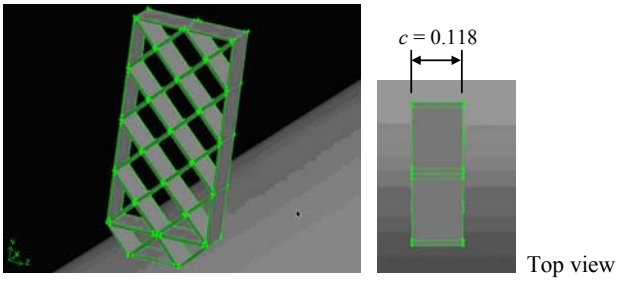

Figure 2. Schematic of the baseline grid fin configuration

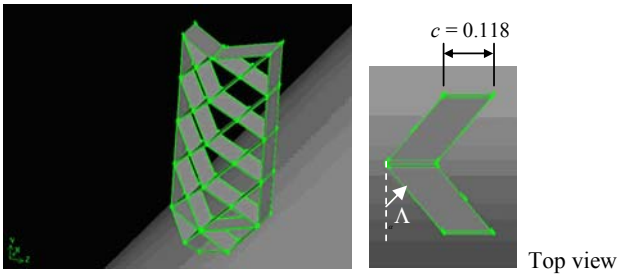

Figure 3. Schematic of the sweptback grid fin configuration

Figure 2 schematically shows the baseline lattice grid fin. The schematic of the proposed improved sweptback grid fin configuration is shown in Figure 3, with the frameworks of grid cells swept back along chord direction while retaining the same projected structure and dimensions as those of the baseline lattice grid fin shown in Figure 1. The sweptback grid fins are also mounted in a cruciform orientation and in the same position on the ogive-cylinder body as the baseline grid fins. The sweptback angle, Λ is 30° in the present study.

B. Mesh generation

The most challenging part in CFD simulations of the flow over a vehicle with grid fins is to create a mesh with satisfactory quality. Due to the complicated geometry of the fins, the structured grid generation requires a lot of manpower. Even if the structured grid can be generated with a lot of time, the quality of the grid distribution may not be good, especially within the region of the grid fins. Thus, in the present study, GAMBIT, supplied in the CFD software FLUENT suite, was used to generate the unstructured grid. Taking advantage of the model symmetry at zero angle of attack, only a quarter of the vehicle with grid fin was considered in the present CFD study.

By exploiting the wall function in FLUENT, boundary layer mesh was used near the vehicle body and fin surfaces. The spacing between the first grid point and the surface is $0.0016D$, with the growth factor of 1.2 and at least 5 rows of boundary layer mesh. In order to enhance the mesh quality, the whole computational domain is divided into three parts: fin part, transitional part and the remaining part. Figures 4(a) and 4(b) show the enlarged grid topology on planes through the fin normal an parallel to the body axis, respectively. Triangle surface mesh can be observed in the fin surface (Fig. 4a). Three transitional parts on the top of, before, and after the fin part are added respectively. With these transitional parts, the very fine mesh in the fin part is gradually transferred into a coarser mesh in the remaining part, which significantly reduces the total number of grid elements of the whole domain. Within these transitional parts, T-Grid type was used, as seen in Fig. 4(b). The advantage of this type of grid is that it allows different grid elements in different surfaces. The disadvantage is that the volume mesh strongly depends on the mesh quality in each surface and thus it is very easy to fail to generate volume mesh due to poor quality of any grid in any surface. In the remaining part, structured grid was used. The total number of grid elements is around 1,500,000 for the whole 3D computational domain of a quarter model and parallel computing was used to speed up the computation.

The grid topology of the sweptback configuration is similar to that for the baseline fin, and it is not shown here for the sake of brevity. Due to its more complex geometry the grid generation for this case was more challenging.

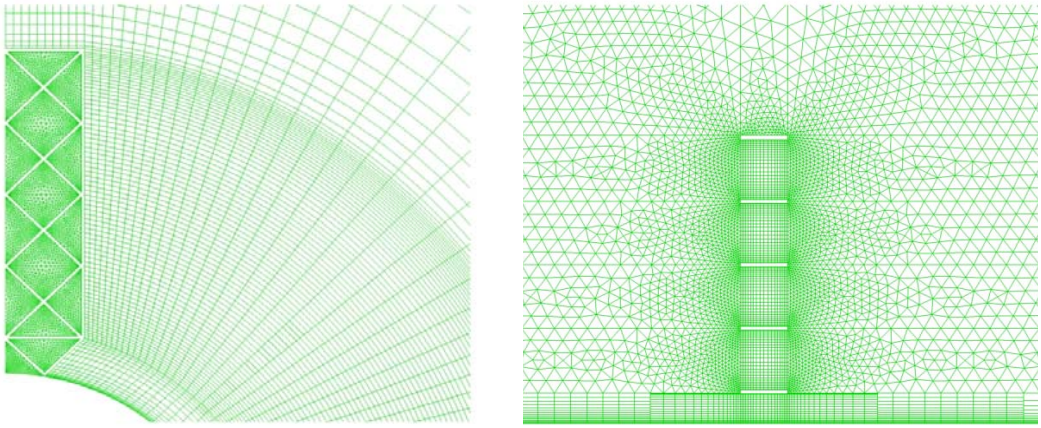

(a) Mesh along a the *y-z* plane across the fin. **(b) Mesh the *x-z* plane across the fin**

Figure 4. Mesh in fin region for the baseline model

C. Numerical method and flow solver

The computation of the flow within the cells of the grid fins is complicated by the complex interaction of the flow and of the shock waves formed from the bluff leading edges. In the present study, 3D Navier-Stokes equations coupled with turbulence model are used to simulate the turbulence field. In this section, the mathematical model and the numerical solution of these models are outlined briefly.

The governing equations for 3D unsteady, compressible, turbulent flow are expressed as follows:

$$\frac{\partial \rho}{\partial t} + \frac{\partial}{\partial x_j}(\rho u_j) = 0 \tag{1}$$

$$\frac{\partial}{\partial t}(\rho u_i) + \frac{\partial}{\partial x_j}(\rho u_j u_i) = -\frac{\partial p}{\partial x_i} + \frac{\partial \hat{\tau}_{ji}}{\partial x_j} \tag{2}$$

$$\frac{\partial}{\partial t}(\rho E) + \frac{\partial}{\partial x_j}(\rho u_j H) = \frac{\partial}{\partial x_j}\left[u_i \hat{\tau}_{ij} + (\mu + \sigma^* \mu_T)\frac{\partial k}{\partial x_j} - q_j \right] \tag{3}$$

where t is time, x_i position vector, ρ the density, u_i velocity vector, p pressure, μ dynamic molecular viscosity. The total energy and enthalpy are $E = e + k + u_i u_i/2$ and $H = h + k + u_i u_i/2$, respectively, with $h = e + p/\rho$ and $e = p/[(\gamma - 1)\rho]$. The term γ is the ratio of specific heats. Other quantities are defined in the following equations:

$$\mu_T = \rho \nu_t \tag{4}$$

$$S_{ij} = \frac{1}{2}\left(\frac{\partial u_i}{\partial x_j} + \frac{\partial u_j}{\partial x_i}\right) \tag{5}$$

$$\tau_{ij} = 2\mu_T\left(S_{ij} - \frac{1}{3}\frac{\partial u_k}{\partial x_k}\delta_{ij}\right) - \frac{2}{3}\rho k \delta_{ij} \tag{6}$$

$$\hat{\tau}_{ij} = 2\mu\left(S_{ij} - \frac{1}{3}\frac{\partial u_k}{\partial x_k}\delta_{ij}\right) + \tau_{ij} \tag{7}$$

$$q_j = -\left(\frac{\mu}{\mathrm{Pr}_L} + \frac{\mu_T}{\mathrm{Pr}_T}\right)\frac{\partial h}{\partial x_j} \tag{8}$$

where δ_{ij} indicates the Kronecker delta.

The CFD software FLUENT was chosen as the flow solver to model the flow phenomena. The governing equations were solved by using finite volume method with unstructured-grid. Spalart-Allmaras one-equation turbulent model was used for simulations. Second-order, upwind discretization scheme was employed for flow variables and turbulent viscosity. Implicit, density-based solver was adopted for high-speed compressible flow investigated in this study.

D. Boundary conditions

The free-stream Mach number (M_∞) range studied is 0.817 ~ 2 and the corresponding Reynolds number (Re_D) is 4.69 ~ 11.48 x 10^5. The free-stream static pressure and temperature are 1atm and 295K respectively. The angle of attack of both the fins and the vehicle with respect to the flow are zero. Far-field pressure boundary conditions were applied for outer radial boundary, symmetry conditions for symmetry surfaces, and non-slip conditions for all solid surfaces. At the downstream outflow boundary a used-defined function program is compiled to extrapolate all the flow quantities including pressure from the interior grid points. Maximum residuals were reduced at least 3 orders of magnitude for all the variables to confirm the global convergence of the simulations.

III. Results and Discussions

A. Validation for baseline model

The aerodynamic drag coefficient C_D, also called axial force coefficients, are calculated by using FLUENT postprocessor to integrate the viscous and pressure forces, along the baseline vehicle model body and fin surfaces. The reference area is 1/4 of the cross-sectional area of the vehicle base, and the reference length is the diameter of the vehicle.

To validate the present numerical approach, the computed drag coefficients of the present CFD study under transonic and supersonic flows with Mach numbers 0.817-2 are compared with the CFD data provided by Orthner et al. [4], as shown in Figure 5. The trends of drag in Figure 5 for all the data are consistent to show that with an increase from a low transonic Mach number to sonic conditions, the drag increases smoothly; and with further increase in Mach number from sonic condition to supersonic condition, the drag decreases gradually. This is believed to be attributed to the flow choking in the lattice grid cells at the transonic conditions.

From Figure 5, it is clear to see that the present results and previous CFD results agree well (within 4%). However, the difference between both CFD results and the experimental ones results is larger (10% or more). This may be due to free flight conditions used in experiments [5], which is quite different from the conditions used in CFD analysis. Nevertheless, both simulations follow quite well the trend of the experimental data indicating that the numerical methods are accurate enough to capture the main flow phenomena and physics of vehicles with grid fins.

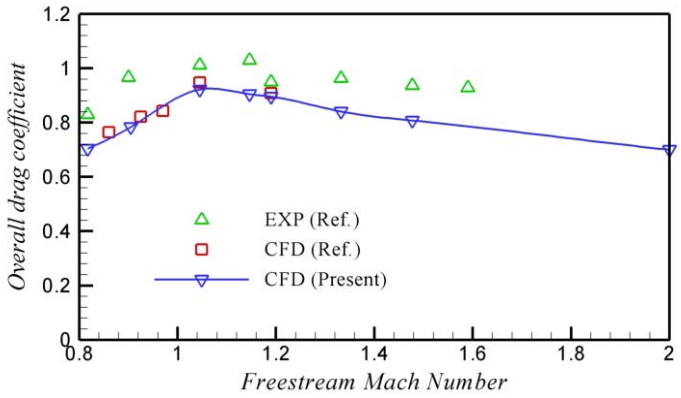

Figure 5. Comparison of the drag force coefficient between present CFD results and given data by Ref. [4]

B. Comparison of aerodynamic drag coefficients between baseline and sweptback models

After validation for the baseline model, the present numerical method is employed to simulate the flows of a vehicle with sweptback grid fins in the transonic and supersonic flows regimes. Similarly, the aerodynamic drag coefficient C_D is integrated along the surfaces of the body and of the sweptback grid fins. The reference length and area are the same as those for the baseline case.

Table 1 and 2 compare the aerodynamic drag coefficients of the overall vehicle equipped with baseline and sweptback fins and of the fins alone

Table 1. Overall vehicle drag coefficient (C_D) with baseline and sweptback grid fins

Freestream Mach number	Baseline grid fin	Sweptback grid fin	Drag reduction
0.905	0.784	0.734	6.38 %
1.045	0.922	0.870	5.64 %
1.190	0.896	0.856	4.46 %
1.332	0.841	0.796	5.35 %
2.0	0.700	0.662	5.43 %

Table 2. Grid-fin drag coefficient ($C_{D,fin}$) for baseline and sweptback configurations

Freestream Mach number	Baseline grid fin	Sweptback grid fin	Drag reduction
0.905	0.504	0.437	13.29 %
1.045	0.448	0.392	12.50 %
1.190	0.406	0.353	13.05 %
1.332	0.384	0.332	13.54 %
2.0	0.345	0.302	12.46 %

The comparisons in Tables 1 and 2 clearly show that the use of sweptback gin fins is beneficial for drag reduction. Table 1 shows that at all the Mach number explored the overall vehicle drag is reduced by 4.46% - 6.38%,by using the sweptback fins in place of the baseline fins. Table 2 shows that the corresponding fin drag reduction is even better with the sweptback configuration having approximately 12.46% - 13.29% less drag than the baseline design. Two main factors are believed to contribute to the drag reduction. First, the slanted surfaces and no-co-planar edges of the sweptback fins is less prone to support the formation of normal shocks (with attendant flow choking) at the back of the lattice cells. Second, these same geometry characteristics favor the formation of oblique shock waves off the leading edges of the lattice which pass more easily through the cells thus improving the flow resistance. This is further elucidated in the following section.

C. Flow characteristics for baseline and sweptback models

The flow fields through the baseline and sweptback grid fin configurations are fairly complex. Figures 6 and 7 show respectively the Mach number (M) and pressure coefficient (C_p) contours on the longitudinal x-z plane passing through a baseline grid fin (left) and sweptback grid fin (right) at the freestream Mach numbers 0.905, 1.19 and 2.0,. The webs have blunt leading edges which cause a rapid expansion of the flow as it passes by the corner. The boundary layer, which grows from the leading edge, coupled with stagnating flow in the web spar junctions introduces a decrease in the flow area, leading to flow acceleration and related choke flow phenomena. As shown in Figures 6 and 7, for the baseline grid fin case, the flow accelerates from the entrance to the exit of the lattice cells inside the lattice cells and reaches pressure values not in balance with the pressure of the flow surrounding the fin. Thus the flow through the cells reaches the pressure of the surroundings through a series of expansions and compressions.

At $M_\infty = 0.905$ and 1.19 the diamond patterns past the lattice elements in Fig. 6 and 7 clearly show the expansion fans of the flow exiting both the baseline and the sweptback grid fins. This expansion to pressure values below the surrounding is followed by a rather abrupt shock across which the flow pressure equalizes to the surroundings. The shocks create an arch past the fin cells whose curvature is small at $M_\infty = 0.905$ (almost normal shock) and more accentuate at $M_\infty = 1.19$. The associate energy dissipation limits an efficient passage of the flow through the lattice (choking). Note that the geometry of the expansion fans and of the shocks at $M_\infty = 0.905$ and 1.19 is similar for the baseline and for the sweptback fins. However the strength of these phenomena and therefore the associated losses are smaller for the sweptback case. Furthermore, at these Mach numbers it is clear that the baseline configuration suffers a higher resistance at the front of the fin where a larger pressure rise is observed at the blunted lattice edges, Fig. 7. The cumulative effect of the phenomena above is a higher drag for the baseline grid fin.

At $M_\infty = 2.0$, i.e. well past the transonic regime, the flow characteristics of the baseline and of the sweptback cases are quite different. The baseline fin suffers high losses from the strong shocks close to the lattice leading edges that coalesce into forming a substantially continuous normal shock attached to the front of the fin. Past this strong shock structure the flow pressure rises at the expense of its energy and the flow emerges at the exit of the cells with relatively low speed and higher pressure than the surroundings. Past the fin an expansion and shock structure similar to the lower speed cases is observed through which the flow pressure equalizes with the surroundings. The shocks in front of the sweptback grid fin are oblique and much weaker than the strong structure of the baseline case. As a result the flow enters the lattice with more energy and establishes a complex high-speed flow pattern within the cells. At the exit of the lattice the pressure distribution of this more complex flow is also unbalanced and undergoes a series of more intricate expansions and compression until reaching the surrounding value. Broadly speaking, it the losses past the sweptback grid-fin seems higher than those of the baseline geometry. However these are more than compensated by the significantly lower losses the sweptback geometry imposes to the flow entering its lattice compared to the baseline case. The net result is lower drag for the sweptback configuration.

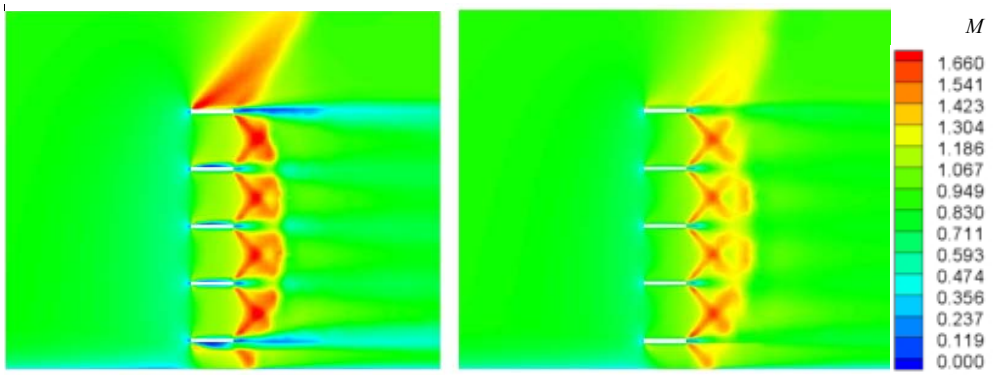

(i) Baseline model **(ii) Sweptback model**

(a) M = 0.905

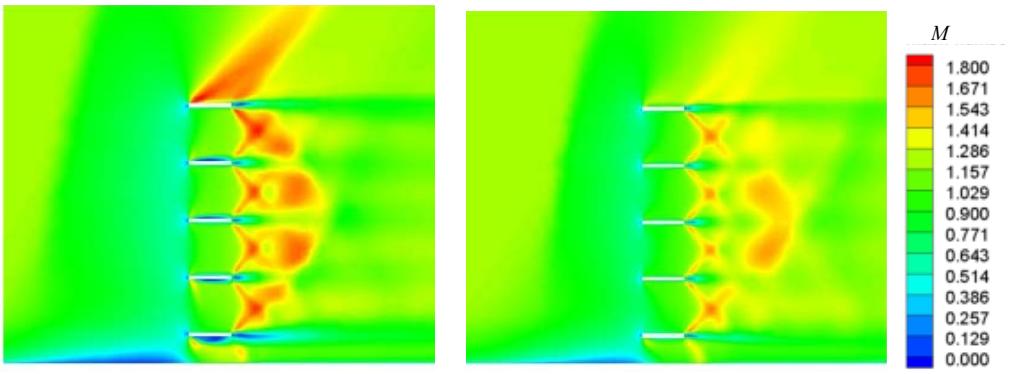

(i) Baseline model **(ii) Sweptback model**

(b) M = 1.19

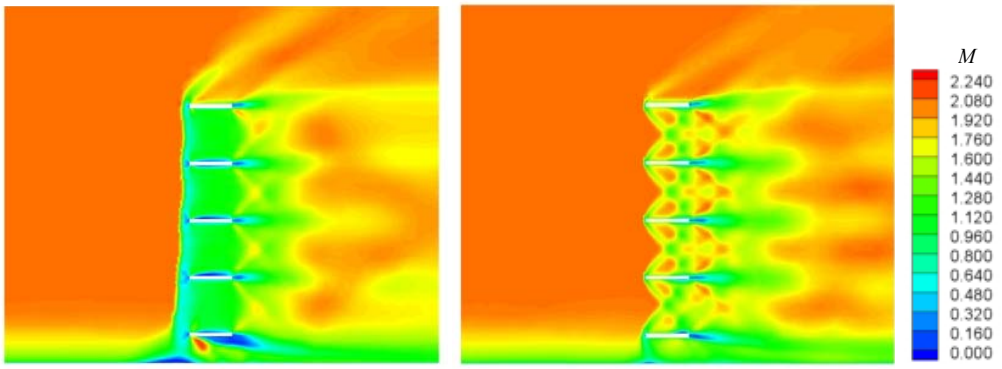

(i) Baseline model **(ii) Sweptback model**

(c) M = 2.0

Figure 6 Mach number contours for the baseline and sweptback models at symmetry surface for freestream M=0.905, 1.19, and 2

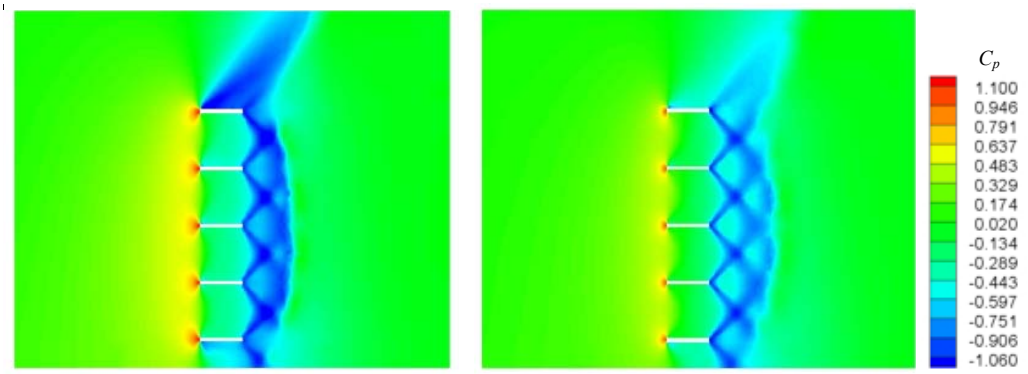

(i) Baseline model **(ii) Sweptback model**

(a) M = 0.905

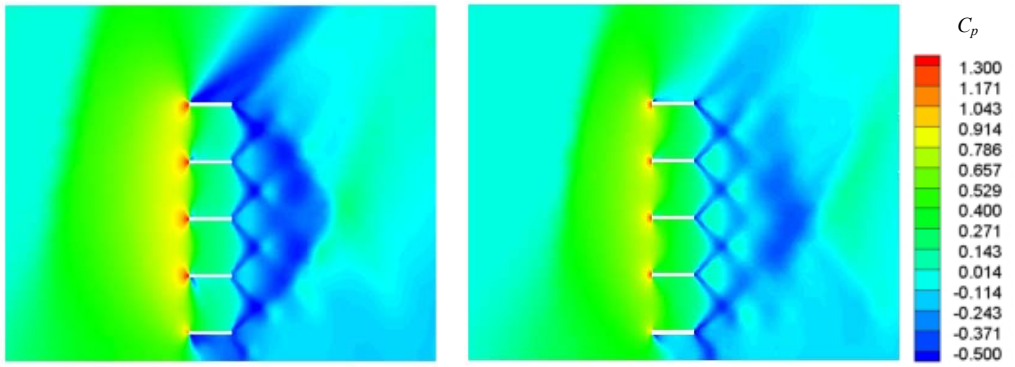

(i) Baseline model **(ii) Sweptback model**

(b) M = 1.19

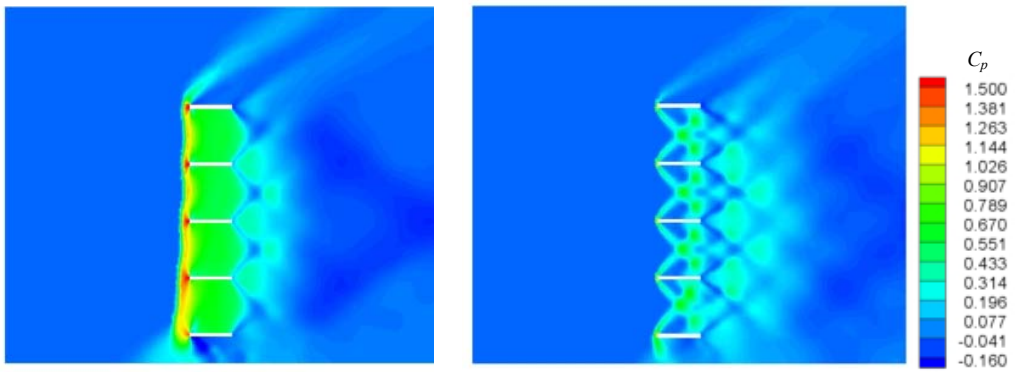

(i) Baseline model **(ii) Sweptback model**

(c) M = 2.0

Figure 7 Pressure coefficient contours for the baseline and sweptback models at symmetry surface for freestream M=0.905, 1.19, and 2

IV. Conclusion

At transonic Mach numbers flow choking usually occurs at the back of the lattice of grid fins, causing a significant increase in drag force. The present study proposes a sweptback grid-fin configuration aimed to to reducing the transonic choking and the associate drag. Viscous computational fluid dynamic (CFD) simulations were performed to investigate flows over an ogive-cylinder with baseline and sweptback grid fins in transonic and supersonic flow regimes in the range of 0.817-2.0, at zero angle of attack. The present simulations show that losses associated to choking and to the formation of shocks in front of the lattice can be reduced by using the sweptback geometry. This translates in a drag reduction of about 5% for the overall vehicle and of nearly 12% for the fins at all the Mach numbers investigated in the present study.

References

[1]Chen, S., Khalid, M., Xu, H., and Lesage, F., "A comprehensive CFD investigation of grid fins as efficient control surface devices," AIAA-2000-987, *38th Aerospace Sciences Meeting and Exhibit*, Reno, NV, Jan. 10-13, 2000.

[2]Lin, H., Huang, J., and Chieng, C., "Navier-Stokes Computations for Body/Cruciform Grid fin Configuration," AIAA-2002-2722, *20th AIAA Applied Aerodynamics Conference*, St. Louis, Missouri, June 24-26, 2002.

[3]Lin, H., Huang, J. C., and Chieng, C., "Navier–Stokes Computations for Body/Cruciform Grid Fin Configuration," *Journal of Spacecraft and Rockets*, Vol.40, No.1, 2003, pp. 30-38.

[4]Orthner, K. S., "Aerodynamic Analysis of Lattice Grids in Transonic Flow," Master's Thesis, Dept. of Aeronautics and Astronautics, Air Force Institute of Technology, Ohio, 2004.

[5]Abate, G., Winchenbach, G., and Hathaway, W., "Transonic aerodynamic and scaling issues for lattice fin projectiles tested in a ballistic range," in proceedings of the 19th International Symposium of Ballistics, pp. 413-420, 7-11 May 2001, Interlaken, Switzerland.